Journal of Geoscience and Environment Protection, 2022, 10, 251-270
https://www.scirp.org/journal/gep
ISSN Online: 2327-4344
ISSN Print: 2327-4336

Effect of Boiling and Cooling of Geothermal Fluids on Precipitation of Secondary Minerals: A Case Study of Olkaria Fields, Kenya

Emmanuel Onesimo Duku[1], Benson G. Ongarora[2], Paul Tanui[2]

[1]Geothermal Energy Training Institute (GeTRI), Dedan Kimathi University of Technology, Nyeri, Kenya
[2]Department of Chemistry, Dedan Kimathi University of Technology, Nyeri, Kenya
Email: eduku96@gmail.com, eduku96@yahoo.com

How to cite this paper: Duku, E. O., Ongarora, B. G., & Tanui, P. (2022). Effect of Boiling and Cooling of Geothermal Fluids on Precipitation of Secondary Minerals: A Case Study of Olkaria Fields, Kenya. *Journal of Geoscience and Environment Protection, 10,* 251-270.
https://doi.org/10.4236/gep.2022.109015

Received: July 21, 2022
Accepted: September 27, 2022
Published: September 30, 2022

Abstract

The main drawback in the utilization of geothermal resources arises from the precipitation of secondary minerals within wells, pipelines, steam separators, turbines and other surface equipment in form of scales. Scale formation is an outcome of the alteration of various rocks dissolved in geothermal fluids that find their way into a reservoir. Once geothermal fluids ascend to the surface, hydrostatic pressure decreases toward a phase separation level that permits the dissolved gases such as CO_2, H_2S and H_2, and steam to separate from the liquid phase by "boiling". Stripping of these volatiles may increase fluid pH, leading to precipitation and deposition of secondary minerals. The study sought to establish the relationship between water-rock interaction and secondary mineral precipitates at the surface and deep fluid at different temperatures during depressurisation boiling and cooling. Samples were collected from selected Olkaria wells; OW-38A, OW-910 and OW-910A. The analysis of the results outlined deep fluid Alkali-Chloride waters and surface steam-heated Alkali-Bicarbonate and acidic Sulphate-Chloride waters. Various models suggested adiabatic boiling, conductive cooling and possible mixing and dilution in the wells. Hydrothermal alteration minerals were found to be in equilibrium with the geothermal fluids at varying temperatures, and the secondary minerals controlled the chemistry of the reservoir. Silica-saturated solutions precipitated silica in OW-910 and OW-910A, which may have resulted from rapid cooling following mixing with cold surface water.

Keywords

Adiabatic Boiling, Aqueous Speciation, Clogging, Conductive Cooling, Depressurisation Boiling, Equilibrium Degassing, Phase Separation, Saturation Index

1. Introduction

The harnessing of geothermal energy resources dates back to ancient times and can broadly be categorised into electricity generation and direct applications. The latter includes use of hot mineral springs and brines for bathing, cooking and heating (Mburu, 2009). Recent advances in technology and the installation of several modern electrical power generating plants presents many opportunities in several countries, tapping this clean and sustainable renewable energy sources. Primary minerals of common rock types stand unstable when in contact with high-temperature fluids of volcanic geothermal systems. They therefore, tend to dissolve in these fluids. Leaching from the rock, boiling and temperature changes, ion-exchange, system composition and precipitation of alteration minerals largely determine secondary minerals formation by changing the system equilibrium (Arnórsson & Bjarnason, 2007). Hydrothermal alteration results in textural, mineralogical and chemical composition changes of a host rock as a consequence of fluid-rock interaction. These fluids change the composition of primary minerals into secondary minerals by adding, removing or redistributing components within variable temperature ranges (Waweru, 2019). In this work, the status of parent rock and geothermal fluids collected from producing wells under conditions of boiling and cooling were investigated. The study also sought to establish the relationship between hydrothermal alteration due to water-rock interaction and secondary mineral precipitates or dissolution at the surface and deep fluid at different temperatures during depressurisation boiling and cooling. The results from this work will contribute to tapping clean and such sustainable renewable energy sources. A series of such studies on a specific well can inform the prediction of the lifespan of the well. Indubitably the probe may unveil a necessity for in-depth studies and analysis of hydrothermal mineral deposits or epithermal precious metal deposits and heavy minerals following phase separation for possible commercial exploitation.

1.1. Background of the Study

Several factors affect hydrothermal alteration and include temperature changes of boiling and cooling fluid, rock permeability, pressure, fluid composition, duration of hydrothermal activity, mineral composition of the primary rocks and chemical changes due to mixing of fluids (Pirajno, 2009). Numerous hydrothermal minerals are deposited within fissures, on wall linings of drilled wells and steam lines that in turn impact reservoir productivity. Throughout any geothermal energy producing wells, changes in temperature, pressure, pH and mineral saturation distract the chemical equilibria of the working fluid and generally lead to scale formation or corrosion. There are three main areas of secondary mineral deposition (Opondo, 2005): deposition from a single-phase fluid (injection pipelines), deposition from flashing fluid (wells, separators, two-phase pipelines) and deposition by steam carryover (separators, steam lines and turbines). When geothermal fluid ascends to the surface, hydrostatic pressure decreases.

Eventually, the pressure drops toward a level that permits the dissolved gases and steam to separate from the liquid phase. This physical process of phase separation is defined as "boiling" (Nicholson, 1993). Additionally, other notable chemical processes that influence the aqueous composition include conductive cooling, dissolution and deposition (precipitation). Adiabatic flashing causes CO_2 stripping and a pH increase, which may lead to calcite scaling. The most common scales consist of calcium carbonate and amorphous silica, but scales of various mineral oxides and sulphides, mostly pyrite, also occur widely (Thomas & Gudmundsson, 1989). The precipitation of calcite from solution is largely due to the effect of steam loss and degassing of CO_2. This relationship is evident in the chemical Equation (1).

$$Ca^{2+}_{(aq)} + 2HCO^{-}_{3(aq)} \rightleftarrows H_2O_{(l)} + CaCO_{3(s)} + CO_{2(aq)} \quad (1)$$

with the head loss provided by the water flow, CO_2 changes to the gaseous state ($CO_{2(aq)} \rightarrow CO_{2(g)}$), which disfavors the $CaCO_3$ dissolution and implies its mineralisation (De Paula et al., 2022). Solubility of silica minerals decreases with a decrease of temperature as opposed to carbonate which is a determinant factor facilitating precipitation of these secondary minerals. The solubility of any silica mineral (quartz, chalcedony etc.) can be presented as shown in Equation (2), below.

$$SiO_{2(s)} + 2H_2O_{(l)} \rightleftarrows H_4SiO_{4(aq)} \rightleftarrows H_3SiO^{-}_{4(aq)} + H^{+}_{(aq)} \quad (2)$$

and the solubility constant is given by; $KSiO_2 \leftrightarrows aH_4SiO_4$.

Silicic acid is a weak acid and dissociates to yield hydrogen ions. If the pH of the solution is increased (becomes more alkaline) then the solubility of silica will also increase as the hydrogen ions are consumed by reaction given in Equation (3).

$$HCO^{-}_{3(l)} + H^{+}_{(aq)} \rightleftarrows H_2CO_{3(aq)} \rightleftarrows H_2O + CO_{2(g)} \quad (3)$$

Deposition of amorphous silica possesses high mechanical strength and is, therefore difficult to remove. This may necessitate an extra cost in maintenance and workover engineering. Highly altered and fractured zones where alteration is dominant are frequently the problematic areas during drilling. These zones are marked by drilling and circulation challenges such as mud loss and pipes getting stuck due to formation slumping (Aldred et al., 1999).

1.2. Location of the Study Area

Olkaria geothermal field is located within the Greater Olkaria Volcanic Complex (GOVC) in the South-Central Kenyan Rift Valley, 125 km northwest of Nairobi city, southwest of Lake Naivasha (**Figure 1**) and along the East African Rift System (EARS) that transects the country from north to south.

To the north the GOVC is bound by Eburru to the north, Longonot to the east, and Suswa to the south (Musonye, 2015). Olkaria geothermal field is a high-temperature geothermal field with temperatures greater than 200˚C. With an estimated resource area of 204 km^2, Olkaria is divided into seven fields for

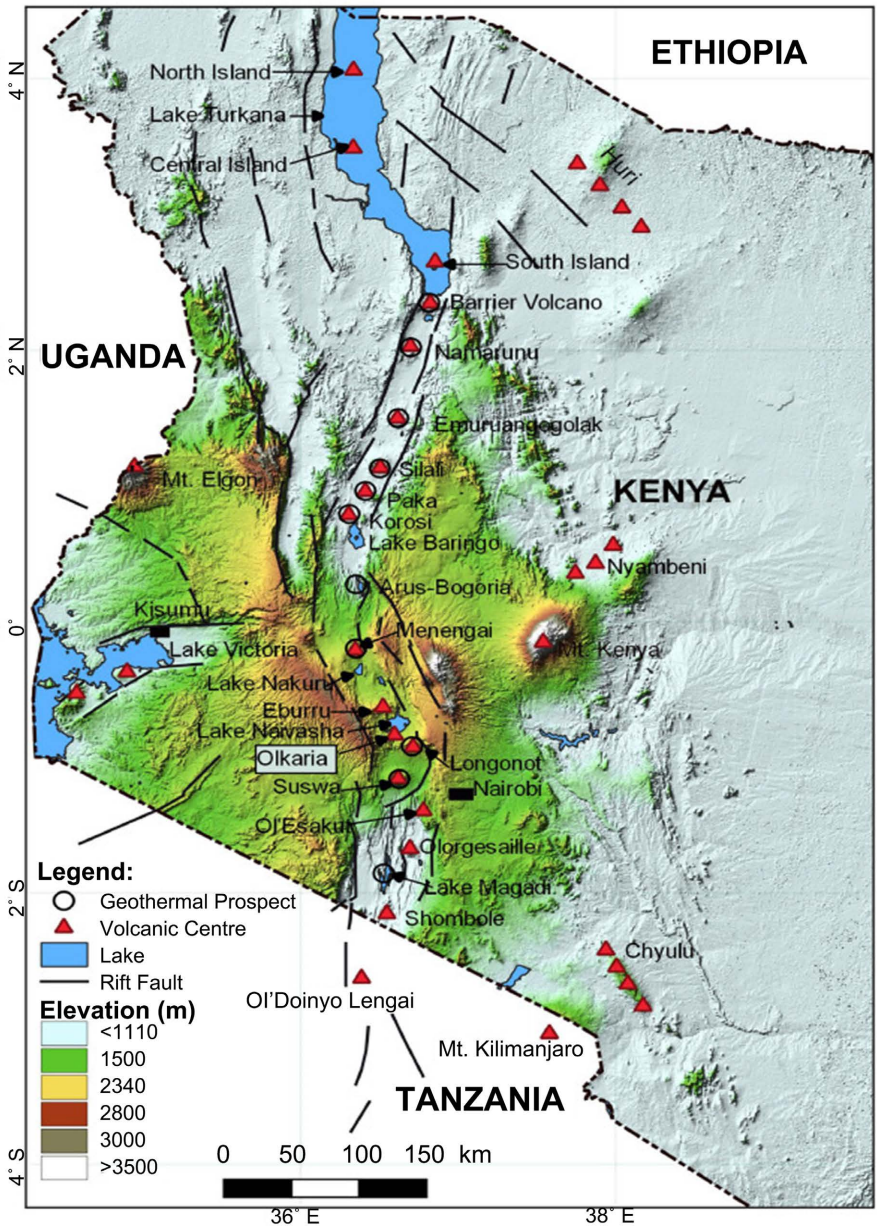

Figure 1. Map of the Kenya rift showing the location of Olkaria geothermal field and other quaternary volcanoes (Omollo et al., 2022).

management purposes. These include the Olkaria Southeast, Olkaria South west, East Production fields, Olkaria Northeast, North-west field Central fields and the Domes fields (**Figure 2**).

Each field is at a different stage of development (Okoo, 2013; Ofwona, 2002). Well, OW-38A is found in the Olkaria East production fields while OW-910 and OW-910A are found in the Olkaria Domes.

1.3. Geology and Tectonic Setting

The East African Rift System, EARS is part of the intra-continental plate divergence rift complex characterised by intense volcanism that took place from late

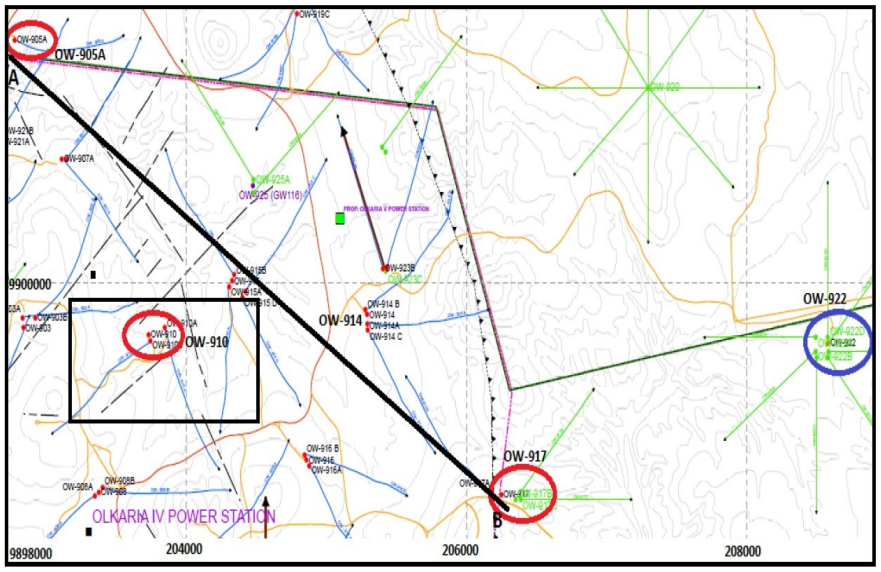

Figure 2. Overview Map showing the sub sectors of the study area (Circled red in black rectangle); OW 910 and OW-910A (Musonye, 2015).

Tertiary to Recent (Macdonald et al., 1992). The Red Sea and the Gulf of Aden are two arms of a postulated triple junction centred on the Afar region. Oceanic crust began to form under these arms since 10 Ma. The third arm, the EARS, extends southwards through Ethiopia, Kenya and Tanzania into Mozambique. The rifting outcome of the African Plate (Nubian plate) from the Arabian plate forms a classic graben averaging 40 - 80 km wide (Simiyu, 2010). Whilst lithospheric extension is occurring beneath the EARS, the rift has not developed to the stage of ocean crust formation. Along the EARS, most volcanic centres had one or more explosive phase including caldera collapse. The volcanic centres host extensive geothermal systems and are spread with hydrothermal activity.

The rifting in the EARS propagated south and separated into the Eastern and Western branches. The western branch extends over a distance of more than 2100 km from Lake Albert (Mobutu) in the north to Lake Malawi (Nyasa) in the south (Chorowicz, 2005). The eastern arm segment of the rift valley, also called the Kenyan Rift System (KRS), extends from Lake Turkana in Northern Kenya (where the earliest volcanic rocks in the Kenyan Rift have been found) to Lake Natron in northern Tanzania (MacDonald, 2002). The Kenyan rift is centred on the hot spot represented by the Kenya dome uplift, which is elliptical in plan and about 1000 km wide. It has three rift arms, two of which form the main rift, whereas the third is subdued, trending west from the centre of the dome (Okoo, 2013). The geology and geological setting of Olkaria geothermal system is entirely in a major volcanic complex that has been cut by an N-S trending normal rifting faults inside the Kenyan rift (Axelsson et al., 2013). This volcanic complex entails at least 80 smaller volcanic centres containing cementite or peralkaline rhyolites. The structural occurrence of these volcanic centres is either steep-sided domes formed out of lava or pyroclastic rock or as thick lava flows. The rocks

within Olkaria geothermal systems are associated with quaternary volcanism and consist of mildly peralkaline silicic volcanic domes, lava flows and the air-fall pumice and peripheral basalts (Omenda, 1998; Lagat et al., 2004). The sub-surface geology of Olkaria consists of a thick volcanic pile of predominantly alkaline, silicic rocks and pyroclastic materials with minor basaltic intercalations (Omenda, 1998).

The structural development in GOVC resulted from the tectonic-thermal rifting and lithospheric thinning during the development of the EARS. The main structures controlling fluid flows include the ring structure, rift fault systems, the Ol'Njorowa gorge, and dyke swarms (**Figure 3**).

The faults trends are ENE-WSW, N-S, NNE-SSW, NW-SE and WNW-ESE. The NW-SE and WNW-ESE faults are thought to be the oldest fault system and they link the parallel rift basins to the main extensional zone (Wheeler & Karson, 1994). Gorge Farm fault is the most prominent of these faults. It bounds the geothermal fields in the north-eastern part and extends to the Olkaria Domes area. The most recent structures are the N-S (Ololbuttot eruptive fissure) and the NNE-SSW faults (Okoo et al., 2017). Outstandingly, subsurface faults have been encountered in most wells drilled in Olkaria. This was proved by drilling problems such as cave-ins and loss of drilling fluid encountered when these faults were dissected during the drilling process (Lagat, 2009).

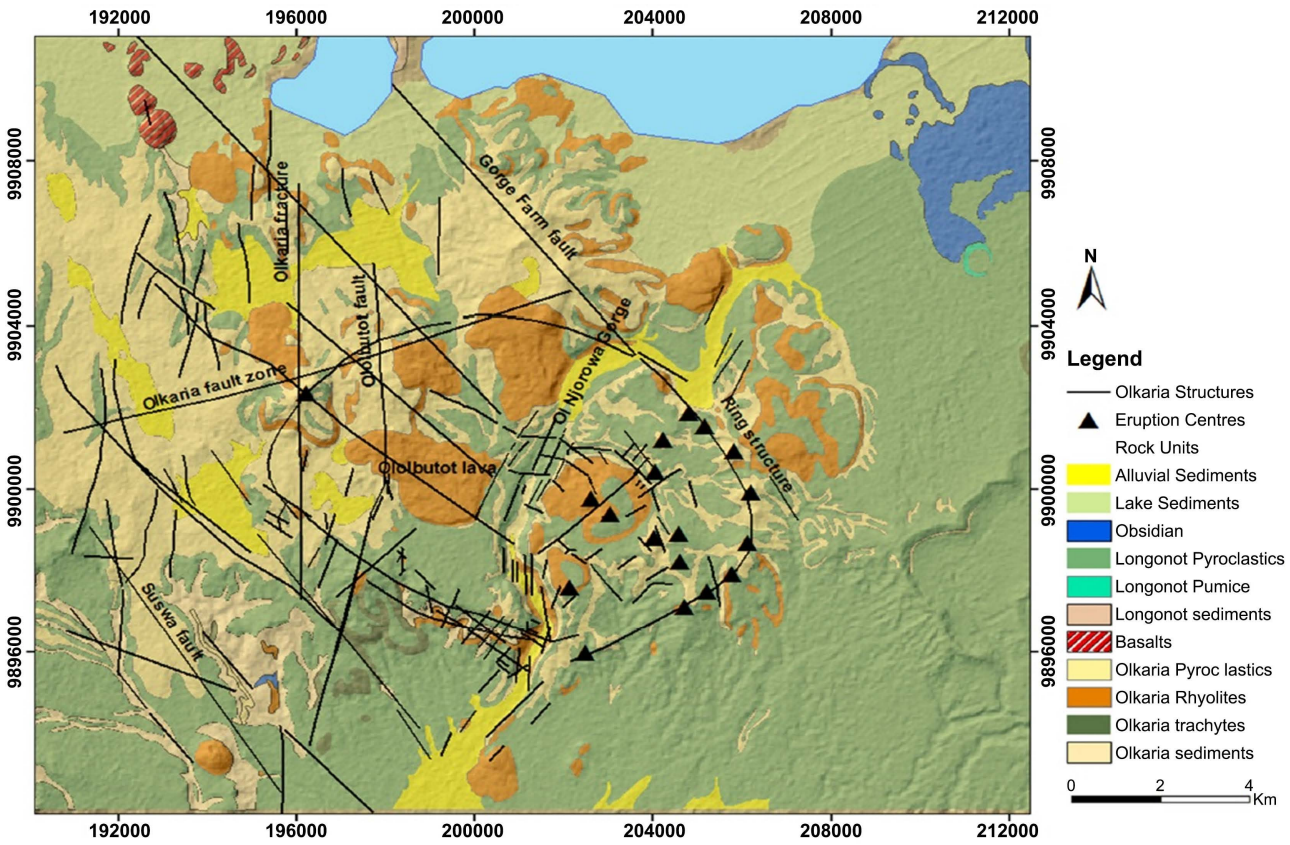

Figure 3. Structural map of the Olkaria geothermal field on detailed geological area (Waweru, 2019).

2. Methods

Geological samples examined in this study were collected from drill bit cuttings by previous geologists during drilling of the wells. Chemical samples were collected during periodic well monitoring under pressure with the aid of a Webre separator connected to a two-phase pipeline close to each geothermal wellhead. The collected samples were composed of water, gas, and mixture of water and steam. Sample collection, treatment and preservations were performed based on recommended procedures of (Arnórsson et al., 2007a; Arnórsson & Ólafsson, 2006). Geological samples were analysed by Binocular and Petrographic microscopy and Powder X-Ray Diffraction (XRD) technique. Geochemical samples were examined by electrometric method for pH, conductivity and TDS; Titrimetric for CO_2, and H_2S; Gas chromatography for N_2, H_2, CH_4, O_2, Ar, and He; Ion chromatography for Cl, B and SO_4^{2-}; Inductively coupled plasma-atomic emissions spectrometry (ICP-AES) for Si, Al, B, Ca, Fe, Li, Mg, K and Na. Complex reactions transpire between aquifer and wellhead during boiling, therefore, a multitude of species required extensive calculations, these were handled by sophisticated WATCH computer speciation programme. The outcome of the WATCH programme (Arnórsson & Hördur, 1982) version 2.4/2010 read input data from chemical analyses of samples collected at surface and generated similar output sample composition which was then used to calculate the composition of aquifer fluids at various temperatures that comprised of pH, aqueous speciation, partial pressure of gases, redox potentials, and activity products based on WATCH geochemical calculations for geothermal applications (Arnórsson et al., 2012). The process was repeated for different temperature ranges of 50˚C, 100˚C, 150˚C, 200˚C, 250˚C, 300˚C, 350˚C, 400˚C and the resultant values were used in the Geochemical aquifer models. Similarly in the steam phase, the WATCH programme computed pH at reference temperature(s) of which were either a fixed value (arbitrary) or a geothermometer temperature calculated by the programme: quartz = 278.0˚C (Fournier & Potter, 1982). Chalcedony = 264.0˚C (Fournier, 1977) and Na/K = 341.8˚C (Arnórsson & Hördur, 1982).

3. Results

3.1. Stratigraphy and Primary Mineralogy

Drill sample analysis uncovered, six primary lithological units: pyroclastics, tuff, rhyolite, trachyte, basalt, and intrusive (**Figure 4**).

The uppermost unit composed of tuff with a matrix of brownish to grey unconsolidated pyroclastics consisting of ash, glass, pumice, obsidian and lithic fragments of weathered lava. This layer is presumed to be part of the upper Olkaria volcanic ranging from a depth of 0 m to 50 m reference to the surface as documented in literature by (Kandie, 2018). Rhyolite was among the dominant strata, rich in silica and composed of mostly light-light brown, greyish-fine grained quartz and feldspar phyric lava. Characterised by moderately altered to greenish and brownish crystalline. Overriding formation in the reservoir rock

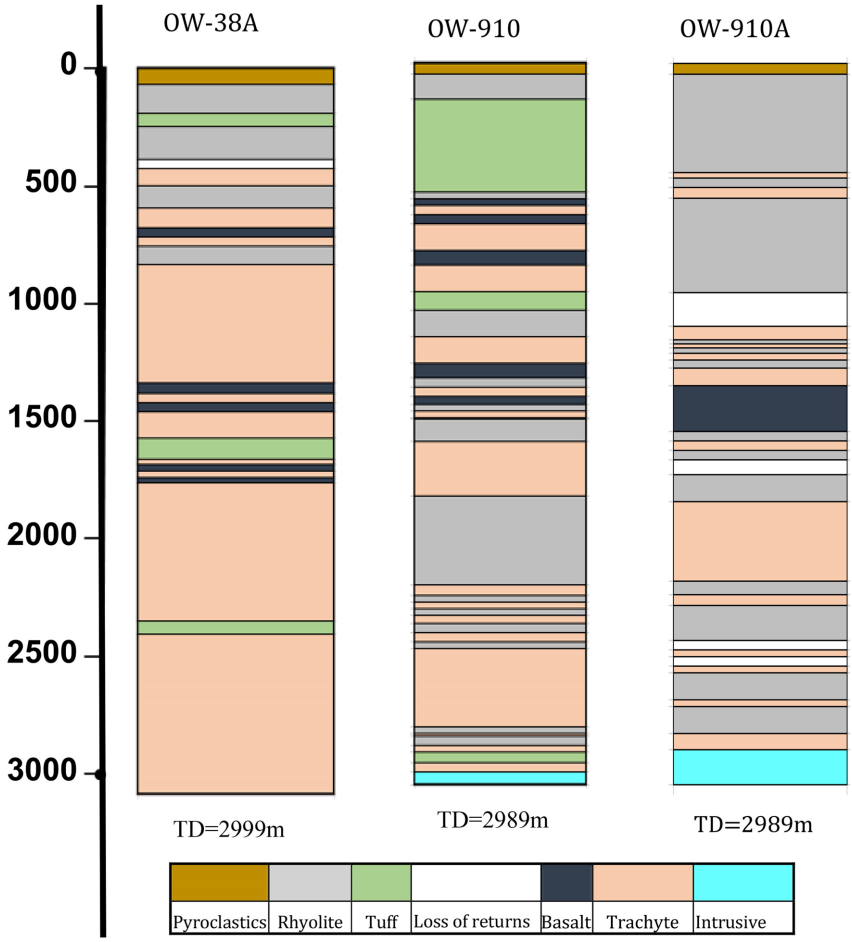

Figure 4. Lithostratigraphic columns of well OW-38A, OW-910 and OW-910A.

was trachyte with quartz and feldspar rich greenish-grey to brownish fine-grained phyric lava. The trachyte displayed moderate to high intensity of alteration to brownish clays. Veined and fractured structures were also observed. Basalt formed the Olkaria geothermal cap rock (Omenda, 1998), which was characterised by dark grey, dark brown fine-grained, highly porphyritic lava with feldspars.

3.2. Secondary Minerals

The main secondary minerals identified included oxides, clays, chloride, calcite, quartz, pyrite and epidote. The overall sequence of alteration minerals investigated from the formation in the wells consisted of:

1) Pyroclastics alteration minerals: chalcedony, oxides.

2) Rhyolite alteration minerals: calcite, chalcedony, chlorite, oxides, pyrite.

3) Trachyte alteration minerals: calcite, chalcedony, chlorite, oxides, pyrite.

4) Tuff alteration minerals: calcite, chlorite, mordenite, oxides, pyrite, quartz.

5) Basalt alteration minerals: calcite, chalcedony, chlorite, epidote, illite, oxides, pyrite, quartz.

Intense and irregular pattern of loss of return have been identified in the wells. This scenario in OW-910A (**Figure 4**) is complemented by abundance of clays

and quartz suggested possible interaction of fluids in the veins with the host rock. The presence of clays, quartz and chlorite has been used as evidence of water-rock interaction (Murakami et al., 1996).

The characteristics of secondary minerals including chlorite, epidote, calcite, pyrite and base metal sulphides highlighted an indication of argillic-propylitic alteration (Table 1). This is probably from the decomposition of basalts, rhyolite and trachytes. Epidote may have correspondingly resulted from the replacement of feldspar in silicic rocks given that albite is known to replace feldspars (Reyes, 2000).

The observed silica (amorphous silica and quartz) in the wells during this study occurs at topmost depth of 1018 m to 2410 m in OW-910 and to nearly total depth (TD) in other wells. Manifestation of quartz suggests silicification (addition of secondary silica). This is confirmed by scale deposits markedly observed at wellhead and steam lines in OW-910A and OW-910 respectively (Figure 5).

Dominant occurrences of clays (smectite, illite, chlorite and calcite) was notable. This could be an indication of acidic or near neutral chemical environment in the geothermal reservoir during equilibration of reservoir fluid with the host rock at various reservoir conditions of alkalinity, temperature and pressure (Velde, 1995).

Table 1. Distribution of altered minerals by depth.

Minerals	Depth (m)		
	OW-38A	OW-910	OW-910A
oxides	0 - 998	0 - 360	0 - 492
clays	50 - 299	0 - 2986	0 - 2788
chlorite	460 - 2174	250 - 2984	188 - 2760
calcite	620 - 2500	586 - 940	1258 - 2700
quartz	1018 - 2410	250 - 2924	1400 - 2640
epidote	1736 - 2344	546 - 2928	972 - 2786
pyrite	1292 - 2999	1356 - 2958	116 - 2732

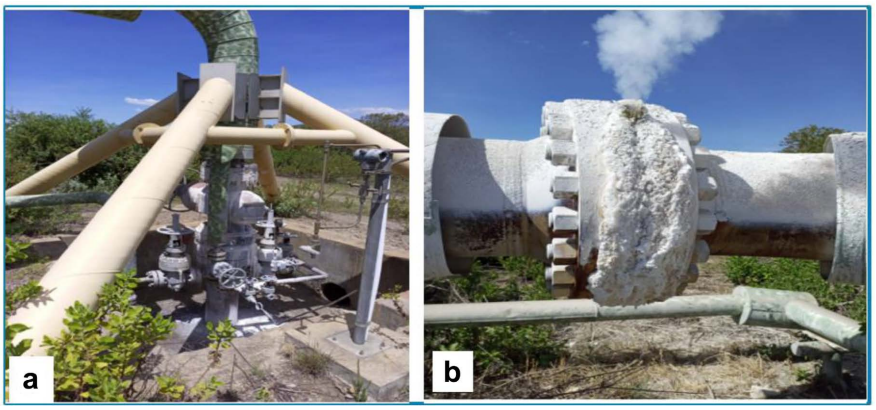

Figure 5. Scale deposition: (a) Wellhead OW-910A; (b) Steam line OW-910.

3.3. Deep-Fluid Chemistry

The composition of the equilibrated sample was calculated on basis of the reservoir having boiled and lost steam before sampling, after single-stage adiabatic boiling and computed fluid sample after conductive cooling. The outcome of the data from chemical analyses of samples collected at surface are recorded in (Table 2 and Table 3).

4. Discussions

4.1. Cation/Proton-Temperature

A mineral solution equilibrium is attained when major elements; cation/proton activity ratios achieve a particular value at a specific temperature. The activity ratios may vary with a different composition from basaltic to silicic volcanic samples. Cation/proton activity ratios of the samples in this study have been plotted against temperature (Figure 6).

The reservoir water shows low Ca^{2+}/H^{+} ratios to Na^{+}/H^{+} and K^{+}/H^{+} activity ratios. Na^{+}/H^{+} and K^{+}/H^{+} activity ratios plot mutually in the equilibrium curve with slight nonconformity. Considering the cation/proton ratios for OW-38A, OW-910 and OW-910A and the fact that K^{+}/H^{+} and Na^{+}/H^{+} ratios are much higher than the Ca^{2+}/H^{+} ratios, aquifer temperatures for the wells under this study are the Na-K geothermometry temperatures of the discharges. This is due to the anomalous concentrations of "indicator" elements in groundwaters and

Table 2. Chemical analyses of water samples collected from discharges of wells OW-38A, OW-910 and OW-910A.

WELLS	GSP (Barg)	WHP (Barg)	Enth. (Kj/Kg)	Cond (μΩ/cm)	TDS (ppm)	Ph	B (ppm)	SO_4 (ppm)	Cl (ppm)	CO_2 (ppm)	F (ppm)	H_2S (ppm)	SiO_2 (ppm)	Ca (ppm)	Li (ppm)	Na (ppm)	K (ppm)	Mg (ppm)
	1.0	4.0	1734	1832	917	9.6	0.83	58.7	250.1	199.3	103.8	0.102	323	1.99	1.21	394.6	35.7	0.225
	2.1	3.6	1815	1966	983	9.9	1.71	63.5	278.2	202.8	104.9	0.51	346	3.02	1.14	460.9	88.1	0.054
OW-910	1.2	3.0	2044	2242	1128	9.8	1.89	60.3	389.4	246.6	122	1.632	341	2.05	1.06	543.6	108.5	0.023
	1.1	2.8	1741	2327	1164	9.3	1.49	86.7	311.4	211.9	124.5	0.544	320	2.51	1.06	535.1	104.6	0.057
	1.0	4.0	1734	1832	917	9.6	0.83	58.7	250.1	199.3	103.8	0.102	323	1.99	1.21	394.6	35.7	0.225
	3.9	7.6	2048	3835	1918	12.3	2.69	210.6	502.3	92.6	220.5	0.952	557	0	2.43	717	380.3	0
	2.2	3.2	1938	2327	1164	9.3	1.49	84.5	419.2	202.4	67.3	1.36	324	1.35	1.07	549.9	107	0.027
OW-910A	2.1	3.6	1815	1966	983	9.9	1.71	63.5	278.2	202.8	104.9	0.51	346	3.02	1.14	460.9	88.1	0.054
	1.2	3.0	2044	2242	1128	9.8	1.89	60.3	389.4	246.6	122	1.632	341	2.05	1.06	543.6	108.5	0.023
	2.2	3.0	2053	1194	2388	9.3	1.89	89.5	410.2	210	64.1	0.34	361	2.22	1.04	554	103.2	0.04
	2.4	5.0	2478	2020	1010	5.2	4.35	314.4	282.2	83.4	59.7	0.34	702	2.2	1.12	367.1	106.3	0.244
	2.5	4.8	2345	2030	1015	6.2	3.74	317.5	361.3	120.6	68.5	0.204	462	2.91	1.15	280	108.9	0.308
OW-38A	1.7	12.0	2604	2376	1188	5.8	0.8	221	214.6	83.4	91.3	0.51	471	2.16	1.46	257.9	47.6	0.126
	4.5	4.8	2576	2324	1162	6.0	0.07	218.2	297.3	109.3	109	0.51	649	1.95	1.41	334.1	96.2	0.163
	2.8	4.5	2610	2898	1444	6.3	0.43	151.2	202.0	150.9	117.5	0.102	344	2.08	1.84	622	75.9	0.099

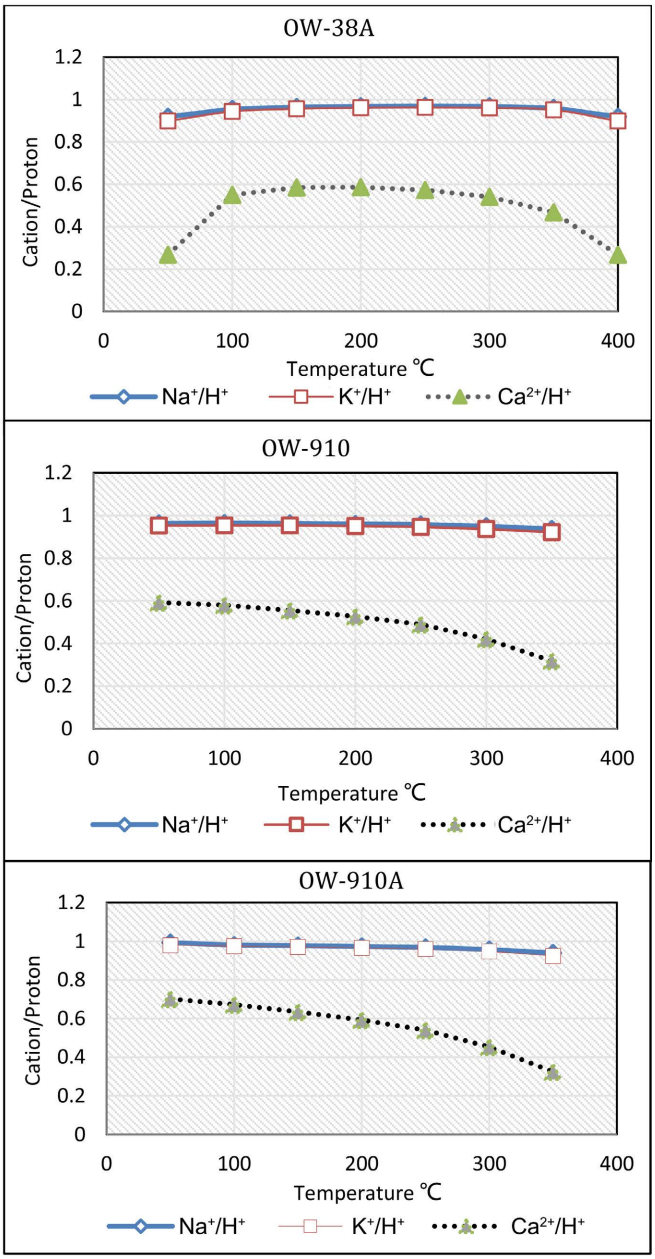

Figure 6. Cation/proton activity ratios for OW-38A, OW-910 and OW-910A.

Table 3. Chemical analysis of steam samples collected from discharges of wells OW-38A, OW-910 and OW-910A.

WELLS	CO_2	H_2S	CH_4	H_2	N_2
	mmoles/100 moles Steam				
OW-910	299.9	0.99	0	2.21	343
	527	2.05	0	6.51	571
	255.7	2.13	0	2.54	104
	723	0.14	0.76	8.5	73.8
	225.3	1.81	0.1	8.77	48

Continued

	130.2	0.86	0.07	1.68	87.2
	143	0.74	0.59	6.96	46.9
OW-910A	527	2.05	0	6.51	571
	255.7	2.13	0	2.54	104
	225.3	1.81	0.1	8.77	48
	492	7.2	0.28	7.51	59.3
	129.5	3.49	0	7.7	55.3
OW-38A	76	3.7	0.01	1.8	8.48
	54.4	1.3	0.04	5.63	8.83
	127.6	4.07	0.07	9.18	9.31

gases samples collected (Fournier, 1977). The overall decline in the trend of activity ratio of Ca^{2+}/H^{+} in the wells with increase in temperature (**Figure 6**) may be attributed to loss of calcium from the ascending solution in the wells as it boils and precipitates calcite (Tarcan, 2001). Therefore, mixed waters tend to be calcite undersaturated and with low Ca^{2+}/H^{+} activity ratios compared with geothermal waters (K^{+} and Na^{+}) which decrease the cation/proton activity ratios (Arnórsson, 1985).

4.2. Enthalpy-Silica

These plots were used to estimate heat and silica balance in the reservoirs and balance of silica with other components on assumptions of no heat loss after mixing, quartz solubility controls the silica content of the reservoir fluid and no dissolution and deposition of silica before and after mixing (**Figure 7**).

Under hydrothermal conditions silica chemistry control phase stability, the trends of enthalpy-silica plots were dispersed between 2000 - 2400 kj/kg and 400 - 800 mg/kg this is due to the solubility of silica in geothermal solutions, silica mixing model and silica geothermometry with adiabatic cooling.

As opposed to enthalpy-SiO_2 plots, Silica-Chloride plots (**Figure 8**) presents a good linear relationship, presumably mixing with no dissolution of silica from the rock and no precipitation had occurred. The trend changed in areas of low Cl concentration. This might be attributed to dilution devoid of boiling. In any case, if unmixed water was in equilibrium with respect to quartz and re-equilibration of the phase occurred after mixing then, considerate silica would have to precipitate from the water.

4.3. Chloride-Boron

High Cl concentration in sample indicates water fed directly from a deep reservoir with minimal mixing or conductive cooling, these are characteristics of groundwater dilution in accordance to (Nicholson, 1993). As observed in **Figure 8(a)** and **Figure 8(b)**.

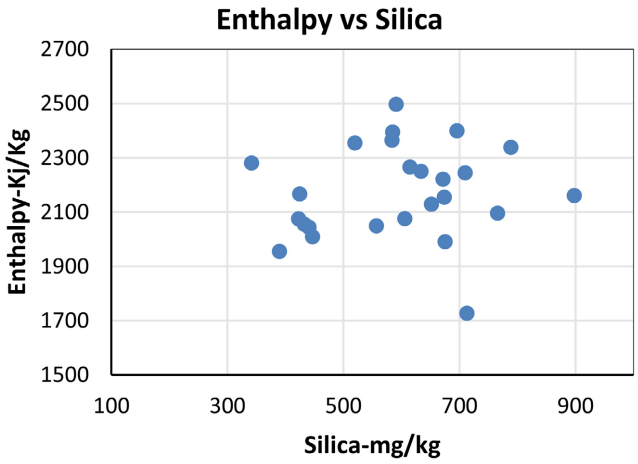

Figure 7. Variation in Enthalpy and the silica content in well discharges of production well OW-910A.

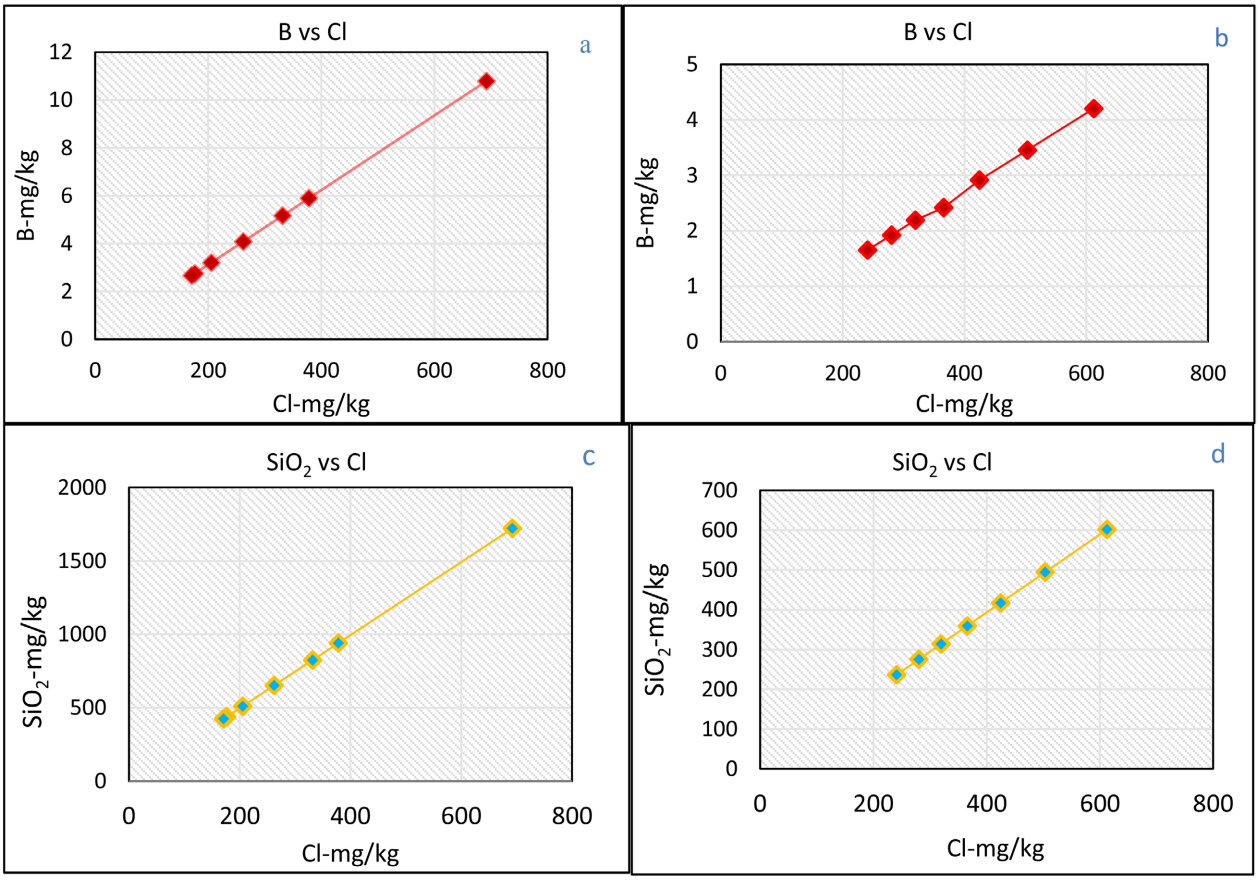

Figure 8. Plot of Chloride with boron and silica in OW-38A and OW-910A: (a) (b) Boron; (c) (d) Silica.

The Cl and B are preservative ions and do not take part in chemical reactions in the reservoir (Arnórsson, 1985). Therefore, Cl and B are not incorporated in the alteration minerals in the reservoir. Most importantly, the concentration of Cl is determined by its concentration in the case of mixing geothermal water with cold water. B/Cl ratios presented a good linear relationship between chlo-

ride and boron concentrations from these wells, with Cl closely in equilibrium with the reservoir water in OW-38A and OW-910. Linear relationship between chloride and bromide constitutes the main evidence for mixing which is further substantiated by, silica and relations (Arnórsson, 1985). The joint of a regression line through the data points at 0 mg/kg boron and chloride for OW-38A and OW-910 (**Figure 8(a)**) indicate a common reservoir source for waters. This is reserved to present strong evidence for mixing geothermal water with cold groundwater and gives the impression of boiling preceding mixing.

4.4. Chloride-Sulphate

Characteristics of steam-heated waters were observed in OW-38A and OW-910A owing to the results from plots in **Figure 8(c)**, **Figure 8(d)** and **Figure 9(a)** and **Figure 9(b)**. This is noticeable by the low Cl and relatively high sulphate concentrations **Figure 9(a)** and **Figure 9(c)**. The positive linear correlation between chloride and sulphate may be due to possible boiling and rise in sulphate resulting from increasing oxidation of the hydrogen sulphide as the fluid ascends. Owing to low pH of the steam heated acid-sulphate waters, there are high chances of acid water effectually dissolving the primary minerals of common rocks leaving a residue rich in amorphous silica, native Sulphur, sulphides and aluminous sulphates (Churchman & Lowe, 2012).

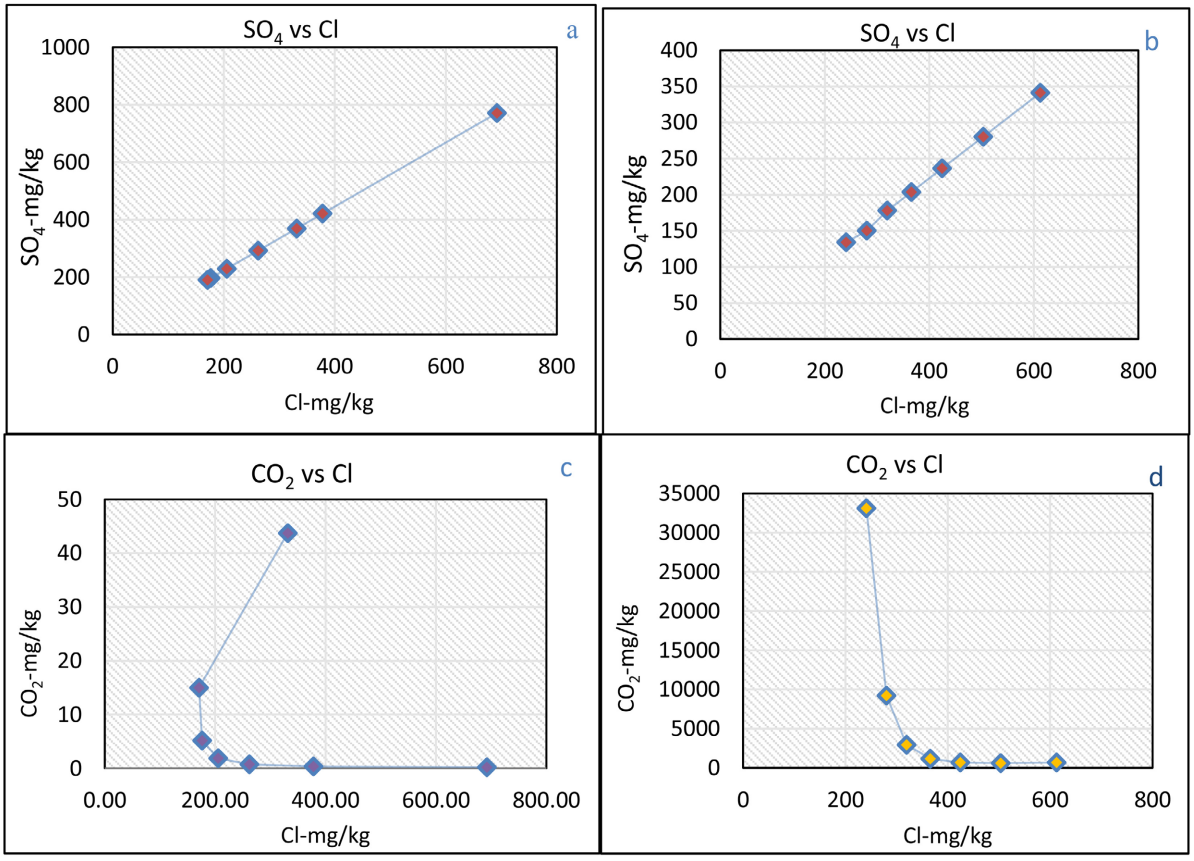

Figure 9. Plot of Chloride with sulphate and bicarbonate OW-38A and OW-910A: (a) (b) Sulphate; (c) (d) Bicarbonate.

4.5. Chloride-Bicarbonate

The wells presented mixing of CO_2 with deep geothermal water in OW-910A Figure 9(c). The probable origin of CO_2 may have been from the mixing of mantle-derived magmatic or metamorphic CO_2 with ground or surface waters from which it is then steam-heated and diluted with shallower water upon boiling (Lowenstern et al., 2015).

4.6. Gas Concentrations and Reservoir Processes

Ideally, volcanic degassing increases the gas concentration in reservoirs, among others including CO_2, H_2S, H_2 and CH_4. The geothermal waters lose part of these gases at the onset of boiling in the reservoir. The reservoir processes considered were boiling and fluid-fluid mixing. The results in the gas concentration of the geothermal fluids in this study were variable with CO_2 being the major constituent at <1% volume, while hydrogen sulphide and hydrogen were relatively abundant. Methane and nitrogen concentrations were variable. Plots of absolute partial gas pressures versus temperatures indicated that the gas pressures increased steadily with temperatures (Figure 10). This is in agreement with kinetic theory with respect to Dalton's and Raoult's laws of partial pressures (Othmer et al., 1953).

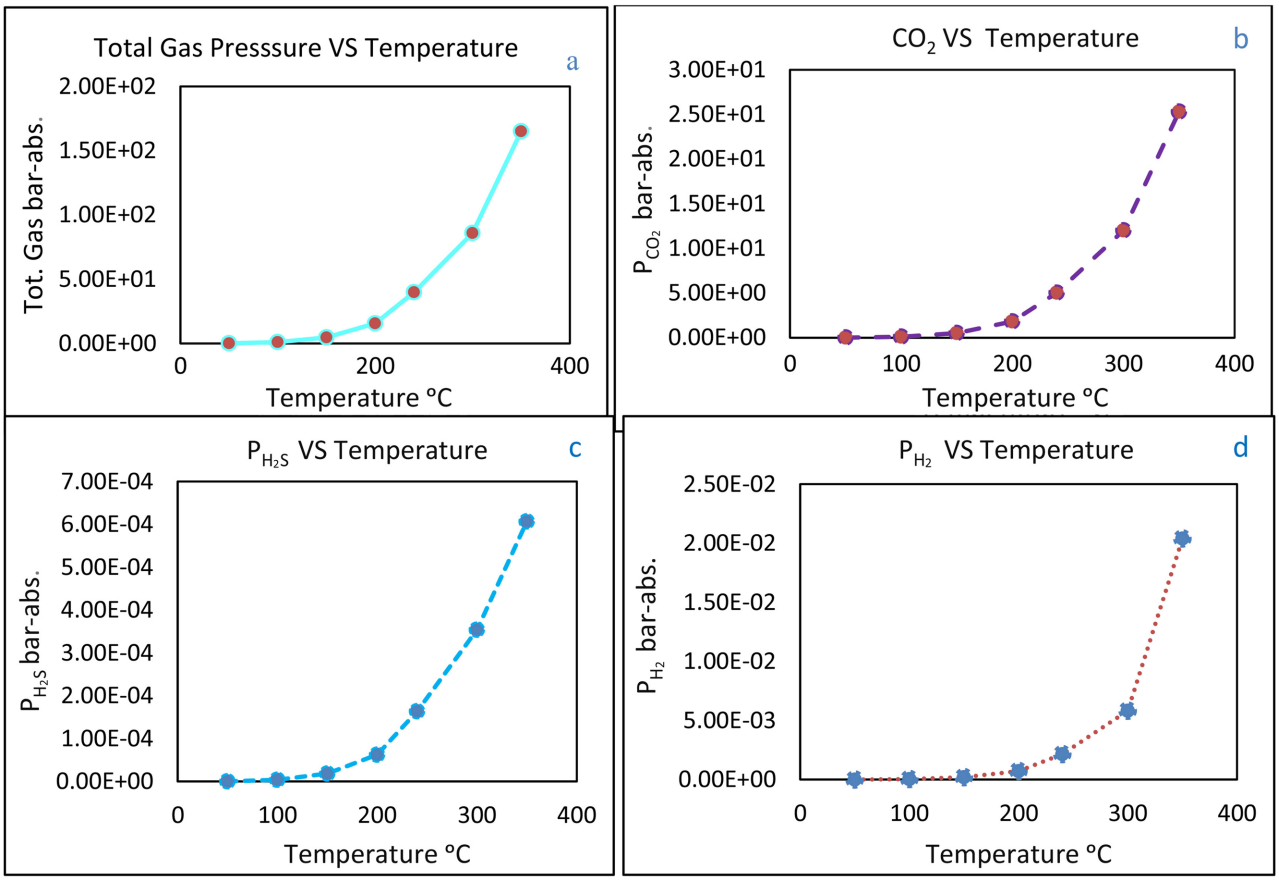

Figure 10. Gas pressures of CO_2, H_2S and H_2 in the aquifer fluid of producing well of OW-910 in Olkaria geothermal field.

4.7. Scaling Potential for Calcite and Amorphous Silica

The state of calcite and amorphous silica saturation was evaluated upon single adiabatic boiling at various temperatures, the computed saturation indices (SI), given by SI = (Log Q/LogK) have been plotted against the temperature of the boiling brine **Figure 10**. The results from the evaluated wells yielded potential calcite and amorphous silica scaling within the wells. The waters are supersaturated with calcite and amorphous silica (positive saturation Indices). However, amorphous silica exhibits more saturation tendencies than calcite (**Figure 11**).

The sharp change in slope of saturation index (SI) between 50˚C and 100˚C in OW-910 (**Figure 11**) may be attributed to the action of degassing of the fluid loss during boiling (Tarcan, 2001). Boiling causes a drastic decrease in CO_2 partial pressures, which leads to calcite oversaturation and precipitation. The oversaturation reaches extreme at a temperature that is a few tens of degrees lower than the temperature at which boiling sets in. At a peak of 100˚C, the water has almost quantitatively been degassed. Continuous boiling, which leads to cooling, will consecutively cause less oversaturation as the solubility of calcite increases with decreasing temperature. In OW-38A, calcite appears to have reached maximum saturation in the fluid and it is evident that decline in solubility is attributed to cooling due to boiling (Simmons & Christenson, 1994).

The solubility of silica can be substantiated at a higher temperature, strong conductive cooling and mixing in up-flow zones may produce undersaturated fluid with a relatively high silica and Na^+/K^+ ratio. Therefore, amorphous silica precipitation is related to water temperature, the degree of water oversaturation and water salinity (Arnórsson et al., 2007b). Consequently, the cooling, which results from boiling, causes the water in the wells to become oversaturated with respect to amorphous silica because its solubility decreases with decreasing temperature. The trend in **Figure 11** indicates amorphous silica is convenient for geothermometric purposes (Arnórsson & Gunnlaugsson, 1985).

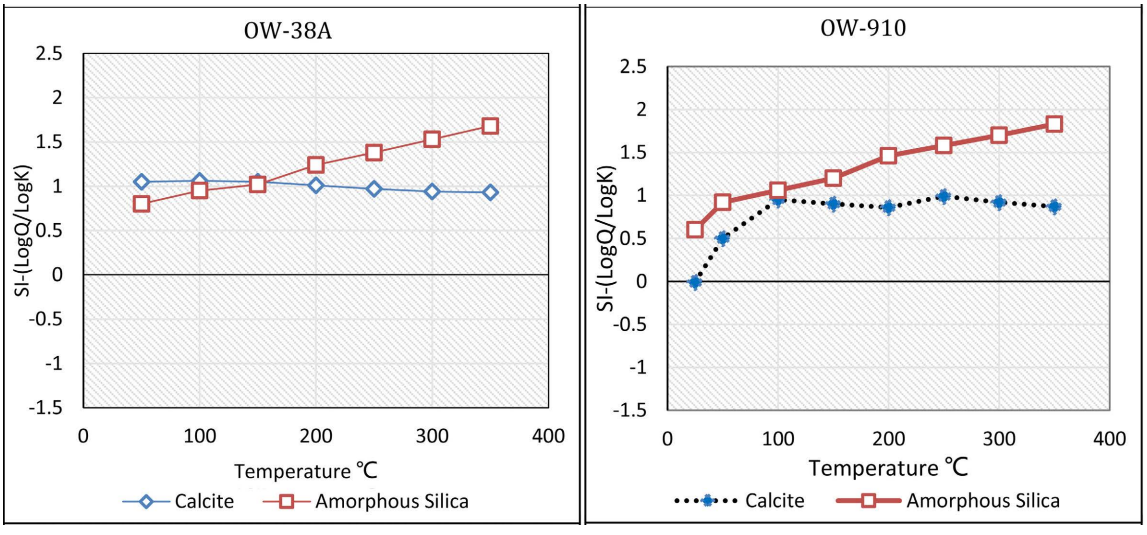

Figure 11. The saturation state of aquifer waters in OW-38A and OW-910 geothermal systems with respect to calcite and amorphous silica.

5. Conclusion

Fluctuations that occurred in temperature and geothermal fluid composition during depressurisation boiling between aquifer and wellhead, largely resulted in changes in mineral saturation. The outcome of such changes was mineral precipitation or mineral dissolution. A comparison was made on the stratigraphy of the wells by correlating their lithologic units, and the outcome showed consistent rock types. The top formation composed of pyroclastics, which overlie rhyolitic lavas with subsequent layers of tuff, trachyte, basalt and intrusive. Basaltic lava flow coincided with the caprock of the reservoir with extrusion of rhyolitic domes whose effects had resulted in minor unconformities.

The resemblance in primary rock composition affirmed the reservoir rocks originated from similar geological regimes with unconformable distribution patterns. Also, the intense and irregular layers at which loss of return occurred in the wells revealed the abundance of clays and quartz; furthermore, this suggested possible alteration zones due to interaction of fluids in permeable zones/ fractures with the host rocks. In addition, the presence of clays, quartz and chlorite confirmed water-rock interaction. The characteristics of secondary minerals of chlorite, epidote, calcite, pyrite and base metal sulphides indicated the possibility of argillic-propylitic alteration, probably from the decomposition of basalts, rhyolite and trachytes. The dominant occurrence of epidote and clays (smectite, illite, chlorite and calcite) might have resulted from the replacement of feldspar in silicic rocks at relatively higher fluid temperatures. Secondary mineral precipitates were observed in drilled wells, wellheads and steam lines in OW-910 and OW-910A respectively. The mineral saturation indices of the geothermal waters were supersaturated with respect to calcite and amorphous silica, indicating that boiling, cooling and dilution had occurred in the wells.

Waters discharged from the wells constituted geothermal fluids of volcanic and meteoric origin that had interacted with various rocks, incorporated dissolved steam and mixed with diluted rain water (surface runoff). The geothermal waters from the discharge wells studied were of three types: alkaline bicarbonate-chloride-sulphate waters. The alkaline-chloride waters were characteristic of the deep geothermal reservoir and the two other groups were secondary fluids notably steam-heated waters from springs. On the other hand, chemical analysis of the fluids from the selected wells indicated that silica, sodium and potassium can be used as geothermometers in Olkaria fields.

Acknowledgements

I am grateful to the German Development Bank (KFW) and the East Africa Community (EAC) through the Inter University Council for East Africa (IUCEA) for the scholarship opportunity at the Dedan Kimathi University of Technology. Special thanks to Kennedy Mativo Kamunya and Victor Otieno at Kenya Electricity Generating Company (KenGen) for supporting my industrial data collection and analysis.

Conflicts of Interest

The authors declare no conflicts of interest regarding the publication of this paper.

References

Aldred, W., Plumb, D., Bradford, I., Cook, J., Gholkar, V., Cousins, L., & Tucker, D. (1999). Managing Drilling Risk. *Oilfield Review, 11,* 2-19.

Arnórsson, S. (1985). The Use of Mixing Models and Chemical Geothermometers for Estimating Underground Temperatures in Geothermal Systems. *Journal of Volcanology and Geothermal Research, 23,* 299-335. https://doi.org/10.1016/0377-0273(85)90039-3

Arnórsson, S., & Bjarnason, J. Ö. (2007). Fluid-Fluid Interaction in Geothermal Systems. *Reviews in Mineralogy & Geochemistry, 65,* 229-312. https://doi.org/10.2138/rmg.2007.65.9

Arnórsson, S., & Gunnlaugsson, E. (1985). New Gas Geothermometers for Geothermal Exploration—Calibration and Application. *Geochimica et Cosmochimica Acta, 49,* 1307-1325. https://doi.org/10.1016/0016-7037(85)90283-2

Arnórsson, S., & Hördur, S. (1982). The Chemistry of Geothermal Waters in Iceland. I. Calculation of Aqueous Speciation from 0 ˚C to 370 ˚C. *Geochimica et Cosmochimica Acta, 46,* 1513-1532. https://doi.org/10.1016/0016-7037(82)90311-8

Arnórsson, S., & Ólafsson, M. (2006). *Collection of Geothermal Fluids for Chemical Analysis*. Iceland Geosurvey.

Arnórsson, S., Bjarnason, J. O., Friðriksson, P., & Oscarson, F. (2012). *Computer Programs in Geothermal Geochemistry*.

Arnórsson, S., Ólafsson, M., & Óskarsson, F. (2007a). *Geothermal Sampling and Analysis.* Short Course II on Surface Exploration for Geothermal Resources, Organized by UNU-GTP and KenGen.

Arnórsson, S., Stefánsson, A., & Bjarnason, J. O. (2007b). Fluid-Fluid Interactions in Geothermal Systems. *Reviews in Mineralogy and Geochemistry, 65,* 259-312. https://doi.org/10.2138/rmg.2007.65.9

Axelsson, G., Arnaldsson, A., Ármannsson, H., Árnason, K., Einarsson, G., Franzson, H., & Hersir, G. P. (2013). Updated Conceptual Model and Capacity Estimates for the Greater Ol Karia Geothermal System, Kenya. In *Thirty-Eighth Workshop on Geothermal Reservoir Engineering Stanford University*.

Chorowicz, J. (2005). The East African Rift System. *Journal of African Earth Sciences, 43,* 379-410. https://doi.org/10.1016/j.jafrearsci.2005.07.019

Churchman, G. J., & Lowe, D. J. (2012). *Alteration, Formation, and Occurrence of Minerals in Soils* (pp. 1-72). CRC Press.

De Paula, C. R., Pereira, F. D. A. R., Soares, E. J., & Ferreira, E. G. (2022). Addressing the Root Cause of Calcite Precipitation That Leads to Energy Loss in Geothermal Systems. *Geothermics, 98,* Article ID: 102272. https://doi.org/10.1016/j.geothermics.2021.102272

Fournier, R. O. (1977). Chemical Geothermometers and Mixing Models for Geothermal Systems. *Geothermics, 5,* 41-50. https://doi.org/10.1016/0375-6505(77)90007-4

Fournier, R. O., & Potter, I. I. (1982). Revised and Expanded Silica (Quartz) Geothermometer. *Geothermal Resources Council Bulletin,* 11, 3-12.

Kandie, R. J. (2018). Borehole Geology and Thermal History of Well OW-737, Olkaria Geothermal Field, Kenya. *Geothermal Training in Iceland, 14,* 187-220.

Lagat, J. (2009). *Hydrothermal Alteration Mineralogy in Geothermal Fields with Case*

Examples from Olkaria Domes Geothermal Field, Kenya. Short Course IV on Exploration for Geothermal Resources, Organized by UNU-GTP, KenGen and GDC, at Lake Naivasha, Kenya.

Lagat, J., Arnorsson, S., & Franzson, H. (2004). Geology, Hydrothermal Alteration and Fluid Inclusion Studies of Olkaria Domes Geothermal Field, Kenya. In *Proceedings World Geothermal Congress 2005* (pp. 1-14). https://www.geothermal-energy.org/pdf/IGAstandard/WGC/2005/0649.pdf

Lowenstern, J. B., Bergfeld, D., Evans, W. C., & Hunt, A. G. (2015). Origins of Geothermal Gases at Yellowstone. *Journal of Volcanology and Geothermal Research, 302,* 87-101. https://doi.org/10.1016/j.jvolgeores.2015.06.010

MacDonald, R. (2002). Magmatism of the Kenya Rift Valley: A Review. *Earth and Environmental Science Transactions of the Royal Society of Edinburgh, 93,* 239-253. https://doi.org/10.1017/S0263593300000420

Macdonald, R., Navarro, J. M., Upton, B. G. J., & Davies, G. R. (1992). Strong Compositional Zonation in Peralkaline Magma: Menengai, Kenya Rift Valley. *Journal of Volcanology and Geothermal Research, 60,* 301-325.

Mburu, M. (2009). Geothermal Energy Utilization. In *Exploration for Geothermal Resources* (pp. 1-11). Kenya Electricity Generating Co., Ltd.

Murakami, T., Isobe, H., Sato, T., & Ohnuki, T. (1996). Weathering of Chlorite in a Quartz-Chlorite Schist: I. Mineralogical and Chemical Changes. *Clays and Clay Minerals, 44,* 244-256. https://doi.org/10.1346/CCMN.1996.0440210

Musonye, X. S. (2015). *Sub-Surface Petrochemistry, Stratigraphy and Hydrothermal Alteration of the Domes Area, Olkaria Geothermal Field, Kenya* (p. 154).

Nicholson, K. (1993). Gas Chemistry. In *Geothermal Fluids* (pp. 87-115). Springer. https://doi.org/10.1007/978-3-642-77844-5_3

Ofwona, C. O. (2002). *A Reservoir Study of Olkaria East Geothermal System, Kenya*. United Nations University, Geothermal Training Programme.

Okoo, J. A. (2013). *Borehole Geology and Hydrothermal Alteration Mineralogy of Well OW-39A, Olkaria Geothermal Project, Naivasha, Kenya* (No. 24, pp. 547-576). Report.

Okoo, J., Omiti, A., Kamunya, K., & Saitet, D. (2017). *Updated Conceptual Model of Olkaria Geothermal Field Naivasha, Kenya*.

Omenda, P. A. (1998). The Geology and Structural Controls of the Olkaria Geothermal System, Kenya. *Geothermics, 27,* 55-74. https://doi.org/10.1016/S0375-6505(97)00028-X

Omollo, P., Nishijima, J., Fujimitsu, Y., & Sawayama, K. (2022). Resistivity Structural Imaging of the Olkaria Domes Geothermal Field in Kenya Using 2D and 3D MT Data Inversion. *Geothermics, 103,* Article ID: 102414. https://doi.org/10.1016/j.geothermics.2022.102414

Opondo, K.M. (2005). *Scale Deposition Experienced in Olkaria Well OW-34*.

Othmer, D. F., Ricciardi, L. G., & Thakar, M. S. (1953). Composition of Vapors from Boiling Binary Systems—New Methods of Representing and Predicting Equilibrium Data. *Industrial & Engineering Chemistry, 45,* 1815-1822. https://doi.org/10.1021/ie50524a057

Pirajno, F. (2009). *Hydrothermal Processes and Mineral Systems*. Springer. https://doi.org/10.1007/978-1-4020-8613-7

Reyes, A. G. (2000). *Petrology and Mineral Alteration in Hydrothermal Systems. From Diagenesis to Volcanic Catastrophes* (77 p.). UNU-GTP, Iceland, Report 18-1998.

Simiyu, S. M. (2010, April). Status of Geothermal Exploration in Kenya and Future Plans

for Its Development. In *Proceedings World Geothermal Congress* (pp. 25-29).

Simmons, S. F., & Christenson, B. W. (1994). Origins of Calcite in a Boiling Geothermal System. *American Journal of Science, 294,* 361-400. https://doi.org/10.2475/ajs.294.3.361

Tarcan, G. (2001). *Aquifer Chemistry and Mineral Saturation in Selected High Temperature Geothermal Areas*. United Nations University.

Thomas, D. M., & Gudmundsson, J. S. (1989). Advances in the Study of Solids Deposition in Geothermal Systems. *Geothermics, 18,* 5-15. https://doi.org/10.1016/0375-6505(89)90004-7

Velde, B. (1995). Composition and Mineralogy of Clay Minerals. In *Origin and Mineralogy of Clays* (pp. 8-42). Springer. https://doi.org/10.1007/978-3-662-12648-6_2

Waweru, K. M. (2019). *Characterization of Hydrothermal Minerals in Up-Flow, Out-Flow and cold In-Flux Zones in Olkaria Geothermal System Using SWIR Hyperspectral Imaging Technique*. Master's Thesis, University of Twente.

Wheeler, W. H., & Karson, J. A. (1994). Extension and Subsidence Adjacent to a "Weak" Continental Transform: An Example from the Rukwa Rift, East Africa. *Geology, 22,* 625-628. https://doi.org/10.1130/0091-7613(1994)022<0625:EASATA>2.3.CO;2